DIFFUSION-LIMITED TUMOUR GROWTH: SIMULATIONS AND ANALYSIS

Philip Gerlee[1]

Center for Models of Life, Niels Bohr Institute
Blegdamsvej 17, 2200 Copenhagen O, Denmark

Alexander R. A. Anderson

H. Lee Moffitt Cancer Center and Research Institute
Integrated Mathematical Oncology
12902 Magnolia Drive, Tampa, FL 33612, USA

(Communicated by Yang Kuang)

Abstract. The morphology of solid tumours is known to be affected by the background oxygen concentration of the tissue in which the tumour grows, and both computational and experimental studies have suggested that branched tumour morphology in low oxygen concentration is caused by diffusion-limited growth. In this paper we present a simple hybrid cellular automaton model of solid tumour growth aimed at investigating this phenomenon. Simulation results show that for high consumption rates (or equivalently low oxygen concentrations) the tumours exhibit branched morphologies, but more importantly the simplicity of the model allows for an analytic approach to the problem. By applying a steady-state assumption we derive an approximate solution of the oxygen equation, which closely matches the simulation results. Further, we derive a dispersion relation which reveals that the average branch width in the tumour depends on the width of the active rim, and that a smaller active rim gives rise to thinner branches. Comparison between the prediction of the stability analysis and the results from the simulations shows good agreement between theory and simulation.

1. **Introduction.** Several recent computational [15, 17, 1, 12] and experimental studies [20, 29, 10] have shown that nutrient limitation is an important factor in determining tumour morphology. Tumours grown in low oxygen concentration have been shown to exhibit complex branched morphologies suggesting that tumour growth under low oxygen concentration occurs through diffusion-limited growth [21], a process which is known to govern the growth of a variety of animate and inanimate systems. This observation could possibly have important implications for cancer treatment as a tumour with a well-defined round margin is easier to surgically remove than one with an irregular morphology. It also suggests that certain modes of treatment such as anti-angiogenic treatment which reduces the oxygen supply to the tumour, actually could make the tumour more invasive.

In this paper we present a hybrid cellular automaton model of tumour growth, aimed at investigating tumour growth in diffusion-limited growth conditions. The model presented herein is a simplified version of a previous model, which also contained an evolutionary component [15]. That model exhibited branched tumour morphologies in low oxygen concentrations, and could also link the oxygen concentration to changes in the evolutionary dynamics. The model presented will not capture the evolutionary side of tumour growth, but its simplicity will allow us to perform a stability analysis, which will give further insight into the dynamics of the model and highlight the impact of the model parameters.

1.1. **Background.** Branched growth patterns have been observed in a variety of different living systems such as bacterial and fungal colonies, and are known to occur when the growth is limited by the diffusion of a nutrient that is necessary for cell division and survival [6, 5]. The morphologies obtained from these living systems resemble that of many non-living systems such as electrodeposition [25], crystal growth [4] and viscous fingers [11, 22]. All of these non-living systems obey the same underlying growth principle, which is that of Laplacian growth, in which the interface between two phases is advanced at a rate proportional to the gradient of a potential field u that obeys Laplace equation $\nabla^2 u = 0$ in one phase and satisifies the boundary condition $u = 0$ at the interface and in the other phase. Depending on the system under consideration the field u represents different physical quantities. In the case of electrodeposition it is the electric field around the substrate, in crystal growth it is the temperature field and in viscous fingering the pressure in the liquid. This growth process is inherently unstable as perturbations to the interface are enhanced through increased flux, and what stabilises the growth are microscopic forces such as the surface tension or capillary force. The growth instabilities that occur in these systems are described by the Mullins-Sekerka instability [28], which shows that the typical length scale of the pattern depends these microscopic parameters of the system under consideration.

This similarity between biological and non-living diffusion limited patterns has led to the hypothesis that the biological patterns could be explained with the same basic principles [24]. Perhaps the most studied example of these biological systems is the growth of bacterial colonies subject to low nutrient levels. Bacteria are usually grown in petri dishes at high nutrient concentrations. These conditions give rise to colonies with simple compact morphologies, but in stressed growth conditions, such as low nutrient concentration or elevated substrate stiffness, morphologies similar to those encountered in diffusion limited growth are observed [24, 26]. Another biological system that displays complex patterns under diffusion limited growth are fungal colonies. Complex branched morphologies have been observed for both multi-cellular filamentous growth [27] and for yeast-like unicellular growth [32]. These patterns primarily arise in low nutrient conditions or when there is a build up of metabolites which inhibit the growth of the tumour.

The diffusion-limited supply of nutrients that occur in the early stages of tumour growth suggests that avascular tumours grow under similar nutrient limited conditions as bacteria cultured in petri dishes. Although the growth of a tumour is a much more complex process compared to the growth of bacteria in petri dishes, the similarity in morphology suggest that tumours exhibit branched morphologies driven by diffusion limited growth. For example, in a clinical study on cervical cancers [20] showed that hypoxic tumours exhibited larger tumour extensions, and similar results have been obtained in *in vitro* studies [29, 10].

1.2. **Previous work.** The connection between low nutrient levels and irregular tumour morphologies has been established in several mathematical models. In a multi-model study by Anderson et. al [3] it was shown that three distinct models all gave rise to fingered morphologies, and that a spectrum of morphologies ranging from compact circular to highly branched emerge depending on the cellular characteristics. Another model by Ferreira et. al [12] also exhibited a range of fingered morphologies, but in this case it was shown that the tumour morphology depends on the concentration of two types of nutrient, one essential for survival and the other necessary for cell division. The above models are all individual-based, but tumour morphology has also been investigated in reaction-diffusion models. The impact of cell-cell adhesion was for example investigated by Frieboes et. al [10]. They show that when the adhesion between cancer cells is low long wave-length perturbations are enhanced and that this can lead to break of of sub-tumours from the main tumour mass. A similar approach was used by Macklin et. al [23]. They found that both the tissue oxygen concentration and the biomechanical properties of the tissue affect the resulting tumour morphology, and in particular that fragmented growth occurs in low oxygen hypoxic conditions.

The model presented in this paper is a simplification of an evolutionary hybrid cellular automaton model which has been used for investigating the impact of the tumour micro-environment on the growth and evolutionary dynamics of tumour growth. In agreement with other models it showed that fingered morphologies occur in low oxygen micro-environments, but more importantly it also established a link between morphology and the phenotypic properties of the cells showing that branched tumour are more likely to contain highly proliferative cells [15]. Extending the model to take into account the extra-cellular matrix further showed that a dense matrix has a stabilising effect on tumour growth reducing the growth rate of small wave-length perturbations and consequently leading to wider branches [17].

2. **The model.** The tissue under consideration is represented by a $N \times N$ cellular automaton with lattice constant Δx. Each automaton element can either be empty or be occupied by a cancer cell and is identified by a coordinate $\vec{x} = \Delta x(i, j)$ $i, j = 0, 1, 2, ..., N - 1$.. This of course neglects the complex interactions between the cancer cells and the host tissue which may contain fibroblasts, macrophages, blood vessels and many other cell types and stimuli, which have all been shown to be important factors in tumorigenesis [31]. However, to keep the model simple we shall focus on tumour cells as the only cell population. The metabolism of cancer cells includes a large number of different chemicals that are all needed for maintenance and cell division, but it is known that the oxygen concentration limits the growth of tumours [33], and we chose to focus on oxygen as the only source of nutrient. The cellular automaton is therefore coupled with a continuous field $c(\vec{x}, t)$ that describes the oxygen concentration in the tissue, and which determines the behaviour of the cancer cells.

Each cell can be in three different states: (i) proliferating, (ii) quiescent and (iii) dead. The cell dynamics are driven by the micro-environment of the cells and if the oxygen concentration falls below a given threshold c_n the cell dies. If the local oxygen concentration is above c_n the cell will be in the proliferative state unless it has more than 3 neighbours (using a von Neumann neighbourhood), in which case it will become quiescent. This mechanism is meant to imitate contact inhibition, a well known characteristic of human cells.

A proliferating cell divides when it has gone through the cell cycle, it then places a daughter cell at random in an empty neighbouring grid point. After cell division has occurred the age of both cells is set to zero, which means that they both need to through the cell cycle again to divide. In order to account for variation in the cell cycle time between different cells it is chosen randomly from a $N(\tau, \sigma)$ normal distribution, where τ represents the average cell cycle time and the variance is set to $\sigma = \tau/2$. For simplicity we have consider non-motile cells, which implies that the growth of the tumour is driven by cell division.

Proliferating cells are assumed to consume oxygen at some fixed rate k, while quiescent cells consume oxygen at a lower rate k_q. Oxygen is assumed to diffuse in the tissue with a diffusion constant D. The nutrient concentration field $c(\vec{x}, t)$ therefore obeys the equation,

$$\frac{\partial c(\vec{x}, t)}{\partial t} = D\nabla^2 c(\vec{x}, t) - n(\vec{x}, t) \tag{1}$$

where $n(\vec{x}, t) = k$ if the automaton element at $\vec{x}$ holds an active cell, $n(\vec{x}, t) = k_q$ if it holds a quiescent cell and $n(\vec{x}, t) = 0$ if it is empty or contains a dead cell. The consumption rates are determined by the per cell consumption rate r_c measured in mol cells^{-1} s^{-1}, together with the well-known fact that $k_q < k$. The boundary conditions satisfied by the nutrient fields are Dirichlet with a constant value c_0. This represents a continuous and fixed supply of nutrient from the boundary of the system, and is meant to imitate a situation where the tissue is surrounded by blood vessels that supply the tumour with oxygen via perfusion.

Please note that as the equation is stated the oxygen concentration can become negative, but this will never happen in a simulation as cell which reside in low oxygen concentration will die, and consequently the consumption term $n(\vec{x}, t)$ will become zero.

This equation is discretised using standard five-point finite central difference formulas and solved on a grid with the same spatial step size as the cellular automaton using an ADI-scheme (please see [17] for details). Each time step of the simulation the nutrient concentration is solved using the discretised equation and all the active cells on the grid are updated in a random order.

In order to make the simulation and analysis of the model simpler we non-dimensionalise the oxygen equation (1) in the standard way. Time is rescaled by the typical time of the cell-cycle, $\tau = 16$ h [8], and the length by the maximal size of a early stage tumour, $L = 1$ cm. The oxygen concentration is rescaled using background concentrations: $c_0 = 1.7 \times 10^{-8}$ mol O$_2$ cm^{-2} [1] and the tumour cell density $n_0 = \Delta x^{-2} = 0.0025^{-2} = 1.6 \times 10^5$ cells cm^{-2} (as the cells reside on a 2-dim. grid) [9]. The new non-dimensional variables are thus given by,

$$\tilde{\vec{x}} = \frac{\vec{x}}{L}, \quad \tilde{t} = \frac{t}{\tau}, \quad \tilde{c} = \frac{c}{c_0}, \quad \tilde{D} = \frac{D\tau}{L^2}, \quad \tilde{r}_c = \frac{\tau n_0 r_c}{c_0}. \tag{2}$$

For notational convenience we have dropped the tildes on the non-dimensional variables.

Cancer cells in multi-cell spheroids are known to consume oxygen at a rate of 4.5×10^{-17} mol cells^{-1} s^{-1} [13] and we therefore set the base oxygen consumption rate to $k = r_c = 4.5 \times 10^{-17}$. The quiescent consumption rate is set to $k_q = k/5$, within the experimentally determined range [13]. The diffusion constant for oxygen is set to $D = 1.8 \times 10^{-5}$cm^2 s^{-1} [18]. The value of c_n is difficult to estimate as it depends on the cell type under consideration, but measurement performed in several

TABLE 1. A summary of parameters in the model.

Parameter	Meaning	Value	Reference
r_c	base oxygen consumption rate	4.5×10^{-17} mol cells^{-1} s^{-1}	[13]
k_q	quiescent oxygen consumption rate	$r_c/5$ mol cells^{-1} s^{-1}	[13]
D	oxygen diffusion constant	1.8×10^{-5} cm^2 s^{-1}	[18]
τ	proliferation age	16 h	[8]
Δx	cell size	25 μm	[9]
c_0	background oxygen conc.	1.7×10^{-8} mol O$_2$ cm^{-2}	[1]
c_n	oxygen threshold	$0.15c_0$	[7]

types of tumours reveal that the oxygen concentration in the necrotic centre of the tumour is 0.5-30% of the concentration in the surrounding tissue [7]. We therefore estimate c_n to be 15 % of the initial oxygen concentration.

A summary of all model parameters can be found in table 1 along with appropriate references. The grid size was set to $N = 200$, which corresponds to a domain size of 0.5 cm and means that we can simulate a tumour of radius 100 cells, which if we assume radial symmetry in a 3-dimensional setting would correspond to a tumour consisting of approximately $100^3 = 10^6$ cells.

2.1. **Simulations.** With this model we have investigated how the oxygen consumption rate k of the cells affects the growth dynamics of the tumour. Note that varying the non-dimensional consumption rate k is equivalent to either varying the dimensional consumption rate or the boundary concentration c_0, see eq. (2). All simulations were started with 4 cells at the centre of the grid and with a homogeneous initial oxygen concentration of $c(\vec{x}, t) = 1$.

Figure 1 shows the spatial distribution of cancer cells for 3 different values of the consumption rate $k = (2r_c, 5r_c, 10r_c)$ after $t = 90$ cell generations. For the lowest consumption rate $k = 2r_c$ the tumour grows with a compact morphology and we observe a wide active region, mostly populated by quiescent cells, surrounding a core of dead cells. This is the typical structure of avascular tumours [33], and is induced by the gradient in the oxygen concentration. For the higher consumption rate $k = 5r_c$ the tumour no longer exhibits a compact shape, but instead grows with a branched morphology where the living cells reside at the tips of the fingers. This phenomena is even more pronounced for $k = 10r_c$, which exhibits thinner branches. These tumour morphologies are similar to those seen in other models of tumour growth [1, 2, 12], and again highlight the importance of the micro-environment in determining tumour morphology. Another phenomenon which is visible is that the branch width seems to depend on the distance to the boundary of the domain. Closer to the centre of the tumour the branches are thinner compared to those at the edge.

3. **Analysis.** We will now proceed to a mathematical analysis of the growth dynamics of the model, similar to the one performed in [16]. The plan is to solve the oxygen equation for a plane tumour interface, then perturb the interface and from
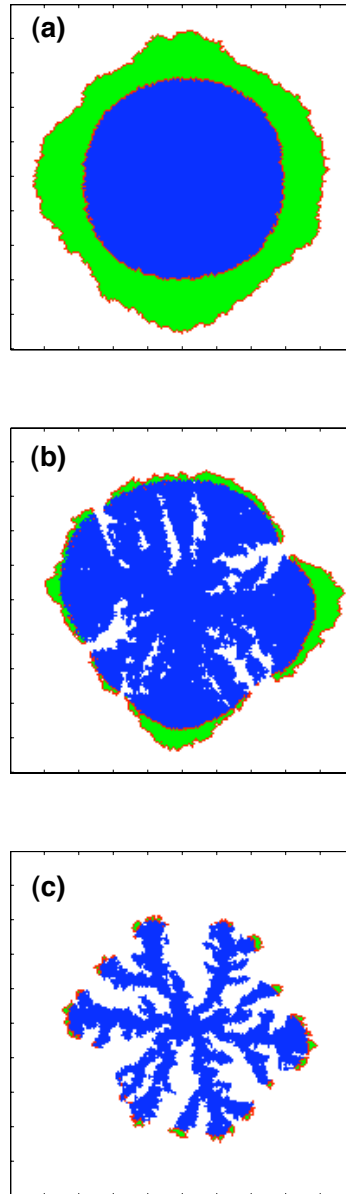
FIGURE 1. The spatial distribution of cancer cells after $t = 90$ cell generations for consumption rates (a) $k = 2r_c$, (b) $k = 5r_c$ and (c) $k = 10r_c$. For the lowest consumption rate the tumour grows with a compact morphology, while for higher k the tumour breaks up into a branched morphology. Note that changing the consumption rate k is equivalent to changing the background oxygen concentration. An interesting observation is that the branches also become wider as they move closer to the boundary of the domain.

that derive a dispersion relation, which describes the growth rate of the perturbation as a function of the wave number. The main assumption for this analysis is that when the oxygen consumption rate of the cells is high compared to the background concentration, the growth of the interface is diffusion-limited, i.e. $v(\vec{x}) \propto \vec{n} \cdot \nabla c$, where $v(\vec{x})$ is the interface velocity and $\vec{n}$ is the normal of the interface [16, 19, 24]. This observation will be the basis for our stability analysis, which means that our treatment of the system will not be rigorously related to our model, but rather aimed more at understanding the dynamics of the model from a qualitative point of view.

3.1. **Sharp interface model.** The oxygen field for the plane interface is found by considering the tumour boundary as a sharp interface stretching infinitely in the y-direction and moving at a constant speed $v_p = \Delta x / \tau$ in the x-direction. The nutrient consumption of the cells is taken to be k in the active part of the tumour, where $c > c_n$, zero in the inactive part, where $c \leq c_n$, and zero outside the tumour. As an approximation we have assumed that the interface is stationary (i.e. $v_p \approx 0$), and try to find the steady-state solution of the nutrient field. This is a reasonable assumption because of the disparity in time-scale between the dynamics of the nutrient field and the movement of the interface (the diffusion time of oxygen across one cell is $\Delta t \approx 4 \times 10^{-3}$ s while cell division occurs on the order of hours). We have assumed that the interface is fixed at a distance S from the domain boundary, and as we are looking for a steady-state solution of the nutrient field this implies that the nutrient equation (1) is reduced to the following set of ODEs:

$$c'' = 0, \quad 0 \leq x < S \tag{3}$$

$$Dc'' - k = 0, \quad S \leq x < S + d \tag{4}$$

$$c'' = 0, \quad x \geq S + d \tag{5}$$

where x is the distance from the domain boundary, S is the distance to the interface and d is the width of the active region of the tumour (where $c > c_n$). We require the solution to be smooth across the interface, i.e. that the solutions to (3) and (4) have the same value as do their derivatives at $x = S$. We also require that the solutions to (4) and (5) take the value c_n at $x = S + d$ and that the derivative is zero at that point. Finally we want the solution to take the value $c(x = 0) = 1$ at the domain boundary. If we let $c_e(x)$ be the external solution, $c_a(x)$ the solution in the active region and $c_i(x)$ in the inactive region we formally require that,

$$
\begin{aligned}
&c_e(0) = 1, \\
&c_e(S) = c_a(S) \\
&c'_e(S) = c'_a(S) \\
&c_a(S + d) = c_i(S + d) = c_n \\
&c'_a(S + d) = c'_i(S + d) = 0.
\end{aligned}
\tag{6}
$$

A solution to (3 - 5) with boundary conditions (6) is given by

$$
c(x) = \begin{cases}
1 - \frac{kd}{D}x, & 0 \leq x < S \\
\frac{k}{2D}\left(x^2 - 2(S + d)x + S^2\right) + 1, & S \leq x < S + d \\
c_n, & x \geq S + d
\end{cases}
\tag{7}
$$

where

$$d = \sqrt{S^2 + \frac{2D}{k}(1 - c_n)} - S \tag{8}$$

is the width of the active region. This solution can now be compared to the simulation results of the full model, though there is one difficulty with this comparison. In the simplified model we assumed that all active cells consume oxygen at a fixed rate k, while in the full model the active rim consists of both proliferating and quiescent cells (see fig. 1), and these cells consume oxygen at different rates. The composition of cells in the active region is difficult to estimate as it depends on the exact geometry and width of the rim. In the comparison with the full model shown in fig. 2, we have estimated the consumption rate to be that of proliferating cells. This is clearly an over-estimate, but still shows good agreement between the analytical result and the oxygen profile obtained from simulation of the full model. The oxygen concentration from the full model is measured radially, which shows that for the tumour sizes we consider the plane interface approximation is reasonable.
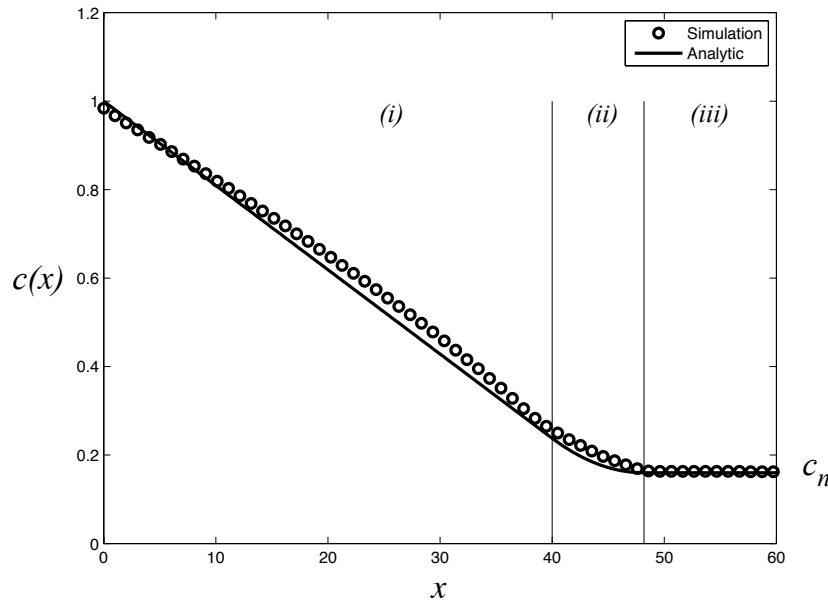

FIGURE 2. The nutrient profile plotted for the bounded domain solution (7) and compared with the radial oxygen concentration of the full model at $t = 60$ when the distance from the domain boundary to the tumour interface is $S = 40$ cells. The solution consists of three parts: (i) outside the tumour, (ii) the active/proliferating region and (iii) the inactive/dead region. The baseline consumption rate is set to $k = 3r_c$.

3.2. **Stability analysis.** We now introduce a small perturbation of wave number q to the interface, which means that the position of the interface is given by $\xi(y, t) = S + \delta(t) \cos qy$. This alters the oxygen concentration in the vicinity of the interface and we need to find the perturb field $c_\delta(x, y)$ to determine the stability of the interface. The steady-state assumption, which made it possible to find unperturbed

oxygen concentration, also simplifies this step of the analysis, as it implies that the nutrient concentration approximately satisfies $\nabla^2 c = 0$ outside the tumour and implies that we can approximate the nutrient profile by a linear function in the vicinity of the interface. Further it allows us to omit any time dependence in the solutions for the perturbed field.

We also assume that the iso-concentration curve $c_\delta(x, y) = c_n$ curve is given by displacing the interface by d in the x-direction, i.e $d(y) = d + \delta \cos qy$ (cf. fig. 3). This is of course only valid when d is small and when the wave number q of the oscillation is small. The values of d which give rise to branching patterns are of the order of one cell size and the interesting range of wave numbers is small as we are not interested in perturbations of wave length smaller than a cell size ($q \leq 2\pi$). This means that this assumption is valid within the dynamically interesting range.
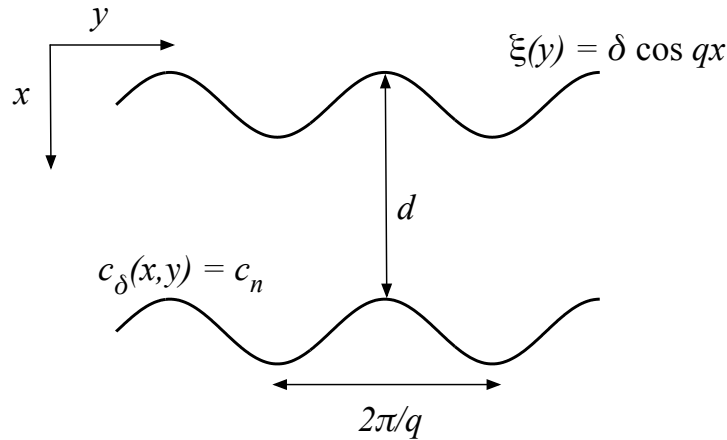

FIGURE 3. This figure shows the structure of the interface. It is assumed that the curve $c_\delta(x, y) = c_n$ is given by displacing the interface by d in the x-direction.

A solution to the oxygen equation for the perturbed interface is given by

$$c_\delta(x, y) = \hat{c}(x) - \delta B e^{-q(S+d-x)} \cos qy. \tag{9}$$

where the linear part $\hat{c}(x)$ is given by

$$\hat{c}(x) = \frac{x(c_n - c(S))}{d} + c(S)\left(1 + \frac{S}{d}\left(1 - \frac{c_n}{c(S)}\right)\right) \tag{10}$$

where $c(S)$ is the concentration at the interface and the constant $B > 0$ is determined from the boundary condition $c_\delta(S + d(y), y) = c_n$. This field satisfies $\nabla^2 c_\delta = 0$ and the boundary condition $c_\delta(S + d(y), y) = c_n$ (to first order in δ) and is therefore an approximate solution for the perturbed interface.

The nutrient field now depends on x and when the consumption rate of cells is large compared to the oxygen concentration at the interface the growth of the interface is as argued above proportional to $\vec{n} \cdot \nabla c_\delta(\xi(y), y)$, where $\vec{n} = (1 + \delta^2 q^2 \sin^2 qy)^{-1/2}(\delta q \sin qy, 1)$. But as $\delta \ll 1$ the interface velocity in the y-direction

is negligible and the gradient dependent growth velocity can be approximated by

$$v(y) = A \left. \frac{\partial c_\delta(x, y)}{\partial x} \right|_{x=\xi(y)} = A \left(\hat{c}'(\xi(y)) + \delta Bq e^{-q(S+d-(S+\delta \cos qy))} \cos qy \right) =$$

$$A \left(\frac{(c_n - c(S))}{d} + \delta Bq e^{-q(d-\delta \cos qy)} \cos qy \right) \tag{11}$$

where $A > 0$ is the constant of proportionality. The velocity can also be written as

$$v(y) = \frac{\partial \xi}{\partial t} = \dot{\delta}(t) \cos qy. \tag{12}$$

Taking the derivative in the y-direction and equating the two expressions for the velocity gives (only taking into account first order in δ)

$$\frac{\partial^2 \xi}{\partial t \partial y} = \left. \frac{\partial^2 c_\delta}{\partial x \partial y} \right|_{x=\xi(y)}$$

$$-\dot{\delta}q \sin qy = -AB\delta q^2 e^{-q(d-\delta \cos qy)} \sin qy \approx -AB\delta q^2 e^{-qd} \sin qy.$$

The growth rate $\dot{\delta}/\delta$ of the perturbation is therefore given by

$$\omega(q) = \dot{\delta}/\delta = ABq e^{-qd} \sim q e^{-dq}. \tag{13}$$

This is the same type of instability we described in [16], where the stability of the growing interface depends on d, the width of the proliferating rim of the tumour. The wave number which has the highest growth rate is $q_{max} = 1/d$, and when d is large only modes with a small wave numbers (long wave lengths, as $\lambda = 2\pi/q$) have a significant growth rate, but for smaller d the maxima is shifted to larger wave numbers (smaller wavelengths) and the growth rates of these wavelengths increase (cf. fig. 4).

3.3. **Comparison to simulations.** We will now proceed to compare the prediction from the stability analysis with the simulation results of the model. In order to do this we must establish a connection between the dispersion relation and a measurable quantity of the tumour, such as the average branch width. When a branch grows it is constantly subject to perturbations and when it reaches a critical width it becomes linearly unstable and splits, similar to what occurs in splitting of viscous fingers [30]. As we do not have any detailed information about the dynamics of the tip splitting we considered a idealised version of the process. We assumed that the branches grow to the critical width $l_c = \lambda_{max} = 2\pi/q_{max}$ at which they split and that each splitting gives rise to two branches of equal width. If we assume that no branches are annihilated and that they grow at a constant speed then an estimate of the average branch width in the colony is

$$l_{avg} \approx (\lambda_{max}/2 + \lambda_{max})/2 = 3/4\lambda_{max} = 3/2\pi d. \tag{14}$$

This is of course a highly idealised picture of the branching process, but at least contains the essential dynamics of the mechanism.

The stability of the interface (and consequently the branch width) depends on a number of model parameters (see eq. (8)), but we have chosen to focus on the consumption rate k and the distance from the boundary S. The reason for this is that changing k is equivalent the background oxygen concentration, an important variable in tumour growth. Secondly, we chose S because it is naturally varied as the tumour grows in the computational domain. It should be noted that the

dimensional parameters (n_0, c_0 etc.) also impact the stability by determining the values of the non-dimensional parameters through eq. (2).

Figure 5 shows the average branch width in the tumour as a function of these two parameters, and from this plot it is clear that the branch width is a decreasing function of both parameters. In order to compare this prediction with the simulation results the average branch width was measured for several values of the oxygen consumption rate and at a range of distances from the domain boundary. The results can be seen in fig. 6, where each measurement was averaged over 30 different simulations and the error bars correspond to one standard deviation.

In comparing the prediction from the stability analysis with the simulation results we again encounter the problem of estimating the consumption rate of the cells. This was resolved by calculating the expected branch width for the two extremes of the cell composition of the active region. In the first case we assume that the rim only consists of quiescent cells with a consumption rate of k_q, and in the other case that the active region only consists of proliferating cells with consumption rate k. This gives us an upper and lower bound on the average branch width in the tumour, and as can be seen from the fig. 6a and 6b this gives a good estimate of the average branch width. Simulations were also performed where all cells (proliferating and quiescent) had the same consumption rate, and the average branch width in this case was in better agreement with the theoretical prediction (data not shown).
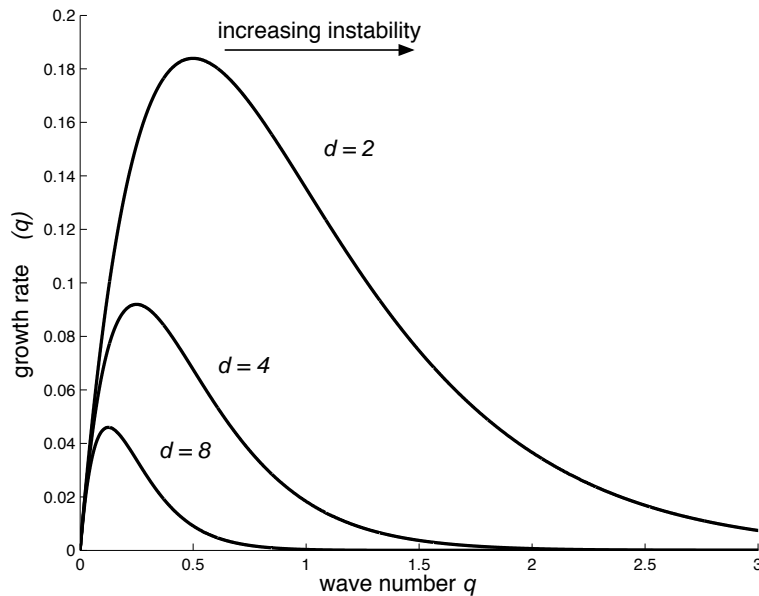

FIGURE 4. This plot shows the dispersion relation (13) for $d = 2, 4, 8$ measured in cell size. It can be seen that both the fastest growing mode and its growth rate depends on the width of the active region d.
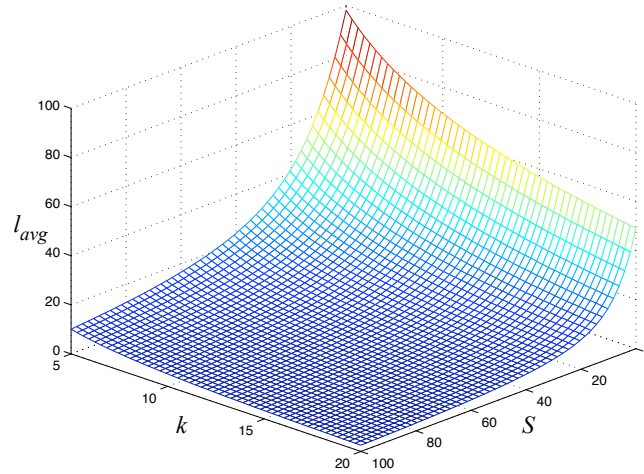
FIGURE 5. The average branch width in the tumour as predicted
by the stability analysis of the bounded domain solution (7). The
branch width is a function of both the distance from the domain
boundary S (measured in cell diameters) and the consumption rate
of the cells k (in units of the oxygen consumption rate r_c, also equiv-
alent to the oxygen concentration). The thinnest branches occur at
a large distance from the boundary and at high consumption rates
(low nutrient concentrations).

As expected the average branch width is a decreasing function of both the con-
sumption rate and the distance from the boundary, although the decrease is more
consistent in the case of the consumption rate. The discrepancy between theory and
simulation when the average branch width is viewed as a function of S is probably
due to the fact that the "distance from the boundary" does not translate well from
one to two dimensions. We made the estimate $S \approx N - R$, where N is the size of
the grid and R is the distance from the centre of the tumour. This clearly under-
estimates the true distance to the boundary, but even more sophisticated methods
cannot give an accurate measure of the distance from the boundary when for ex-
ample screening effects are involved, or when the width of a branch is on the order
of the distance from the boundary.

From the data in fig. 6a we also calculated the consumption rate which best
reproduces the branch width in the simulation. This was found to be approximately
$2k/5$, and using this value we can calculate the fraction of quiescent and proliferating
cells in the active region. The average consumption rate in the active region is given
by

$$k_{avg} = n_q \frac{k}{5} + n_p k \qquad (15)$$

where n_q, n_p are the fraction of quiescent and proliferating cells which satisfy $n_q +
n_p = 1$. We know that $k_{avg} = 2k/5$, and from this we can calculate the fraction of
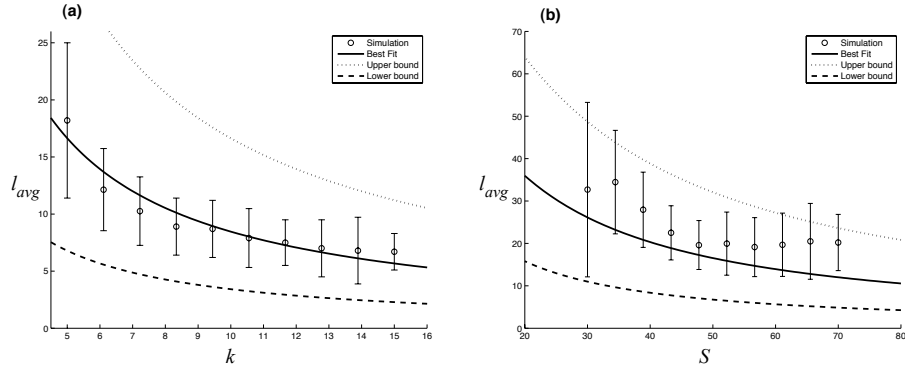quiescent cells to be $n_q = 3/4$.

FIGURE 6. The average branch width in the full model as a function of (a) the consumption rate (or equivalently the oxygen concentration) and (b) the distance from the boundary. The results from the full model are shown in circles and the lines represent different estimates of the consumption rate of the cells in the active region of the tumour. Each measurement was averaged 30 times and the error bars correspond to one standard deviation. In the figures S and l_{avg} are given in terms of cell size and the consumption rate k is normalised with the baseline consumption rate r_c. In figure (a) the branch width was measured at a distance of $S = 50$ and in (b) the consumption rate is $k = 5$. The dotted line shows the predicted branch width if the consumption rate is that of quiescent cells ($k = r_c/5$), while the dashed line corresponds to the consumption rate of proliferating cells ($k = r_c$). The solid line shows the best fit to the data in (a) and corresponds to a consumption rate of $k = 2r_c/5$.

4. **Conclusions.** In this paper we have presented a simple hybrid cellular automaton model of tumour growth aimed at investigating the branched morphologies observed in a number previous models [15, 1, 12]. The cell dynamics in this simplified model are reduced to cell proliferation and nutrient consumption, but the model still exhibits complex branched growth patterns. Simulation results show that consumption rate (or equivalently the oxygen concentration) affects the growth dynamics, and that under low consumption rates the tumour grows with a compact morphology while for higher consumption rates we observe branched growth. Biologically this means that we expect to find tumours with a well-defined margin in a well oxygenated tissue, while a harsh micro-environment with a poor vasculature is likely to produce tumours with a branched morphology. Although branched morphologies are generally associated with aggressive tumours, it should be noted that the tumour mass is smaller in the low oxygen case which could result in a lower tumour burden.

By observing a separation in time-scales between the growth of the tumour and the dynamics of the oxygen field we could derive an approximate solution of the oxygen equation, which showed good agreement with the simulation results. Under the assumption that in low oxygen concentrations the growth of the tumour is diffusion-limited we could then derive a dispersion relation, which describes the

stability of the tumour interface. The stability analysis showed that the average branch width critically depends on the width d of the active region, which acts as a buffer for perturbations to the tumour interface. When d is large the growth is stable and we observe compact tumours, while for smaller d the growth becomes unstable and this leads to branched tumour growth.

The width of the active region depends on several parameters, but most importantly on the consumption rate k (or equivalently the oxygen concentration) and the distance from the boundary S. The fact that low nutrient levels leads to branched tumour growth has been previously observed in several mathematical models [2, 12, 10], but the stability of the growth has never been associated with the width of the proliferating rim. The theoretical result was compared to the simulations by measuring how the average branch width in the tumour depends on the consumption rate k and the distance from the boundary S. This comparison showed good agreement between theory and simulation, and also gave insight into the composition of cell types in the active rim of the tumour.

The stability analysis also allows us to estimate the impact of other model parameters such as the nutrient diffusion constant D and the hypoxia threshold c_n. If we consider the width of the boundary layer as a function of the diffusion constant D, then we can see that the average branch width scales as $l_{avg} \sim \sqrt{D}$ (as $l_{avg} \sim d$). The dependence on D is especially relevant in the case of glycolytic tumours [14], where the growth of the tumour is limited by glucose instead of oxygen. The diffusion of glucose is approximately 5-fold faster than oxygen, and this implies that a tumour which is dominated by glycolytic cells should exhibit wider branches. This phenomenon was in fact observed in [17], and is something that could be tested experimentally. Similarly we see that $l_{avg} \sim \sqrt{1 - c_n}$, which suggests that tumours consisting of cells with a down-regulated apoptotic response to hypoxia (i.e. smaller c_n) should exhibit wider branches. These observations could offer new ways of determining cellular characteristics in a tumour by simply inspecting the morphology. According to this prediction wider fingers should be correlated with the existence of glycolytic cells and cells with reduced hypoxia-induced apoptosis. This observation poses a difficulty in that these two characteristics (glycolysis and reduced hypoxia) usually are associated with poor prognosis, while at the same time they, according to our model, stabilise tumour growth. This means that there could be several factors influencing tumour morphology, and that these in turn can affect the outcome of the disease in different directions.

In conclusion we have presented simulations and analysis of a hybrid cellular automaton model of tumour growth. Our findings highlight the importance of the micro-environment of the tumour and in particular the oxygen concentration, which we could directly relate to the resulting tumour morphology. These findings shed new light on the dynamics of diffusion-limited tumour growth, and will hopefully increase our understanding of the progression of the disease.

REFERENCES

[1] A. R. A. Anderson, *A hybrid mathematical model of solid tumour invasion: The importance of cell adhesion*, Math. Med. Biol., **22** (2005), 163–186.
[2] A. R. A. Anderson, A. M. Weaver, P. T. Cummings and V. Quaranta, *Tumor morphology and phenotypic evolution driven by selective pressure from the microenvironment*, Cell, **127** (2006), 905–915 doi: 10.1016/j.cell.2006.09.042.
[3] A. R. A. Anderson, K. A. Rejniak, P. Gerlee and V. Quaranta, *Mirconevironment driven invasion: A multiscale multimodel investigation*, J. Math. Biol., In review, (2008).

[4] E. Ben-Jacob and P. Garik, *The formation of patterns in non-equilibrium growth*, Nature, **343** (1990), 523–530.

[5] E. Ben-Jacob, I. Cohen and G. L. Gutnick, *Cooperative organization of bacterial colonies: From genotype to morphotype*, Annu. Rev. Microbiol., **52** (1998), 779–806.

[6] E. Ben-Jacob, I. Cohen and H. Levine, *Cooperative self-organization of microorganisms*, Advances in Physics, **49** (2000), 395–554.

[7] J. M Brown and W. R. Wilson, *Exploiting tumour hypoxia in cancer treatment*, Nature, **4** (2004), 437–447.

[8] P. Calabresi and P. S (eds) Schein, "Medical Oncology 2nd edn.," McGraw-Hill, New York, 1993.

[9] J. J. Casciari, S. V. Sotirchos and R. M. Sutherland, *Variation in tumour cell growth rates and metabolism with oxygen-concentration, glucose-concentration and extra-cellular ph*, J. Cell. Physiol., **151** (1992), 386–394.

[10] V. Cristini, H. B. Frieboes, R. Gatenby, S. Caserta, M. Ferrari and J. Sinek, *Morphologic instability and cancer invasion*, Clin. Cancer Res., **11** (2005), 6772–6779.

[11] G. Daccord, J. Nittmann and H. E. Stanley, *Radial viscous fingers and diffusion-limited aggregation: Fractal dimension and growth sites*, Phys. Rev. Lett., **56** (1986), 336–339.

[12] S. C. Ferreira, M. L. Martins and M. J. Vilela, *Reaction-diffusion model for the growth of avascular tumor*, Phys. Rev. E, **65** (2002), 021907.

[13] J. P. Freyer, E. Tustanoff, A. J. Franko and R. M. Sutherland, *In situ consumption rates of cells in v-79 multicellular spheroids during growth*, J. Cell. Physiol., **118** (1984), 53–61.

[14] R. A. Gatenby and R. J. Gillies, *Why do cancers have high aerobic glycolysis?* Nat. Rev. Cancer, **4** (2004), 891–899.

[15] P. Gerlee and A. R. A. Anderson, *An evolutionary hybrid cellular automaton model of solid tumour growth*, J. Theor. Biol., **246** (2007), 583–603, a.

[16] P. Gerlee and A. R. A. Anderson, *Stability analysis of a hybrid cellular automaton model of cell colony growth*, Phys. Rev. E, **75** (2007), 051911, b.

[17] P. Gerlee and A. R. A. Anderson, *A hybrid cellular automaton model of clonal evolution in cancer: The emergence of the glycolytic phenotype*, J. Theor. Biol., **250** (2008), 705–722.

[18] J. Grote, R. Susskind and P. Vaupel, *Oxygen diffusivity in tumor tissue (ds-carcinosarcoma) under temperature conditions within the range of 20–40 degrees c*, Pflugers Arch., **372** (1977), 37–42.

[19] D. Hartmann and T. Miura, *Modelling in vitro lung branching morphogenesis during development*, J. Theor. Biol., **242** (2006), 862–872

[20] M. Höckel, K. Schlenger, B. Aral, M. Mitze, U. Schaffer and P. Vaupel, *Association between tumor hypoxia and malignant progression in advanced cancer of the uterine cervix*, Cancer Res., **56** (1996), 4509–4515.

[21] D. A. Kessler, J. Koplik and H. Levine, *Pattern selection in fingered growth phenomena*, Advances in Physics, **37** (1988), 255–339.

[22] K. J. Måløy, J. Feder and T. Jøssang, *Viscous fingering fractals in porous media*, Phys. Rev. Lett., **55** (1985), 2688–2691.

[23] Paul Macklin and John Lowengrub, *Nonlinear simulation of the effect of microenvironment on tumor growth*, J. Theor. Biol., **245** (2007), 677–704.

[24] M. Matsushita and H. Fujikawa, *Diffusion-limited growth in bacterial colony formation*, Physica A, **168** (1990), 498–506.

[25] M. Matsushita, M. Sano, Y. Hayakawa, H. Honjo and Y. Sawada, *Fractal structures of zinc metal leaves grown by electrodeposition*, Phys. Rev. Lett., **53** (1984), 286–289.

[26] M. Matsushita, J. Wakita, H. Itoh, K. Watanabe, T. Arai, T. Matsuyama, H. Sakaguchi and M. Mimura, *Formation of colony patterns by a bacterial cell population*, Physica A, **274** (1999), 190–199.

[27] S. Matsuura and S. Miyazima, *Self-affine fractal growth front of aspergillus oryzae*, Physica A, **191** (1992), 30–34.

[28] W. W. Mullins and R. F. Sekerka, *Morphological stability of a particle growing by diffusion or heat flow*, Journal of Applied Physics, **34** (1963), 323–329.

[29] S. Pennacchietti, P. Michieli, M. Galluzzo, M. Mazzone, S. Giordano and P. M. Comoglio, *Hypoxia promotes invasive growth by transcriptional activation of the met protooncogene*, Cancer Cell, **3** (2003), 347–361.

[30] L. Ristroph, M. Thrasher, M. B. Mineev-Weinstein and H. L. Swinney, *Fjords in viscous fingering: Selection of width and opening angle*, Phys. Rev. E, **74** (2006), 015201.

[31] H. Rubin, *Microenvironmental regulation of the initiated cell*, Adv. Cancer Res., **90** (2003), 1–62.

[32] T. Sams, K. Sneppen, M. H. Jensen, C. Ellegaard, B. Eggert Christensen and U. Thrane, *Morphological instabilities in a growing yeast colony: Experiment and theory*, Phys. Rev. Lett., **79** (1997), 313–316.

[33] R. M. Sutherland, *Cell and environment interactions in tumor microregions: The multicell spheroid model*, Science, **240** (1988), 177–184.

E-mail address: `gerlee@nbi.dk`
E-mail address: `Alexander.Anderson@moffitt.org`